RSC Advances

PAPER

View Article Online
View Journal | View Issue



Cite this: *RSC Adv.*, 2024, **14**, 16801

# Facile one-pot synthesis of the mesoporous chitosan-coated cobalt ferrite nanozyme as an antibacterial and MRI contrast agent†

Abolghasem Abbasi Kajani, *[ab] Ali Pouresmaeili [a] and Mehdi Kamali[bc]

Cobalt ferrite (CoFe) nanoparticles (NPs) with appropriate physicochemical and biological properties have attracted great attention for biomedical applications. In the present study, chitosan-coated mesoporous CoFe (CoFeCH) NPs were synthesized using a facile one-step hydrothermal method and fully characterized using FE-SEM, EDS, BET, FTIR spectroscopy, DLS, TGA, XRD, and VSM. The spherical, highly colloidal, and monodispersed CoFeCH NPs with an average hydrodynamic size of 177.9 nm, PDI of 0.238 and zeta potential value of −33 represented a high saturation magnetization value of 59.37 emu $g^{-1}$. $N_2$ adsorption–desorption analysis confirmed the mesoporous structure of CoFeCH NPs with a type IV isotherm, calculated specific surface area of 89.583 $m^2$ $g^{-1}$ and total pore volume of 0.3668 $cm^3$ $g^{-1}$. CoFeCH NPs exhibited high antibacterial effects on *S. aureus* and *E. coli*, comparable with standard antibiotics, while CH-coating led to higher biocompatibility of CoFe NPs on human cells *in vitro*. CoFeCH NPs also showed significant peroxidase activity with a $K_m$ value of 14.37 and specific activity of 0.632 mmol $min^{-1}$. CoFeCH NPs were successfully used as a MRI contrast agent with an $R_2$ value of 91.3 $mM^{-1}$ $s^{-1}$. The overall results indicated the high potential of synthesized CoFeCH NPs by the present method for biomedical applications, especially as an antibacterial and MRI contrast agent.

Received 1st April 2024
Accepted 12th May 2024

DOI: 10.1039/d4ra02462a

rsc.li/rsc-advances



## 1 Introduction

Materials at the nanoscale usually display novel physicochemical and biological properties that cannot be observed at bulk scales. Among these properties, the optical, electrical, magnetic, catalytic, antioxidant and antimicrobial properties have been more considered in the biomedical fields.[1] A wide range of enzyme activities including catalase, oxidase, and peroxidase have also been reported for different nanoparticles (NPs).[2–4] The synthesis of NPs with novel and superior enzyme activities is one of the active and cutting-edge fields of research owing to their high stability, low cost, and ability of large-scale synthesis.[5] These NPs with mimical enzyme properties are known as nanozymes, while studying the kinetics of nanozymes is a new and interesting field known as nanozymology.[6]

In this context, the effect of size, shape, and composition of NPs on their enzyme activities have been studied and reported recently.[7–9] The addition of transition metals such as Co, Mn, Ti and Cr to the magnetite structure has been reported to increase the nanozyme activity of the resultant NPs.[10] Among them, cobalt ferrite (CoFe) NPs have been considered for different biomedical applications such as magnetic drug delivery, radio frequency, hyperthermia, magnetic resonance imaging (MRI), and medical diagnostics owing to their properties including chemical and mechanical stability, wear resistance, and ease of synthesis.[11–13] However, the potential toxicity of CoFe NPs significantly limits their biomedical applications, which makes their surface functionalization necessary with biocompatible biomolecules such as organic polymers.[14,15]

Nowadays, the emergence of multiple drug resistance (MDR) and the extension of microbial diseases due to the widespread application of antibiotics are among the main concerns of human health.[16] Antimicrobial resistance is expected to cause about 10 million deaths by 2050.[17] Therefore, the discovery of alternative agents to antibiotics for the treatment of infections is an urgent need.[18] Regarding the different action mechanisms of NPs compared to antibiotics, which is mainly *via* the direct effects on the bacterial cell wall, NP-mediated disinfection has attracted great attention.[19] The development of efficient antimicrobial nanozymes could be a promising solution to this problem, and nanozymes with peroxidase-like activity are of great use for this purpose.[17] The reactive oxygen species (ROS) generated by these nanozymes in the presence of $H_2O_2$ can oxidize the bacterial membranes, thereby reducing the infection.[20] Moreover, the magnetic NPs can also display the antimicrobial activity by heat generation under an alternating

[a]*Department of Biotechnology, Faculty of Biological Science and Technology, University of Isfahan, Isfahan 81746-73441, Iran. E-mail: agh.abbasi@bio.ui.ac.ir; agh.abasi@gmail.com; Fax: +98-3137932342; Tel: +98-3137934401*

[b]*Environmental Research Institute, University of Isfahan, Isfahan, 81746-73441, Iran*

[c]*Department of Environmental Engineering, University of Tehran, Tehran, Iran*

† Electronic supplementary information (ESI) available. See DOI: https://doi.org/10.1039/d4ra02462a

magnetic field, a phenomenon well known as magnetic hyperthermia.[21] Chitin and its deacetylated derivative, chitosan (CH), are frequently found in the exoskeleton of insects, crabs and shrimps. The availability, biocompatibility, biodegradability, antimicrobial activity, and many reactive functional groups of chitin derivatives have made them suitable for different biomedical purposes.[22] Therefore, they are extensively used for the surface functionalization of NPs to improve their physicochemical properties as well as creating new properties.[23]

In the present study, the mesoporous and highly monodispersed CH-coated CoFe (CoFeCH) NPs were synthesized by a facile and one-pot hydrothermal method and their physicochemical properties were fully characterized. Then, the biocompatibility and potential antibacterial activity of CoFe and CoFeCH NPs were studied and confirmed *in vitro*. Finally, the high peroxidase-like activity of CoFeCH NPs was elucidated and their potential application as an MRI contrast agent was reported for the first time.

# 2 Materials and methods

## 2.1. Materials

Dimethyl sulfoxide (DMSO), ferric chloride hexahydrate ($FeCl_3 \cdot 6H_2O$), cobalt chloride hexahydrate ($CoCl_2 \cdot 6H_2O$), low molecular weight CH (product # 448 869, $M_W$ = 50–190 kDa, degree of deacetylation [DD] = 75–85%), sodium acetate ($CH_3COONa$, NaAc), ethylene glycol, glacial acetic acid ($CH_3COOH$, 99%), ethanol, and hydrogen peroxide ($H_2O_2$, 30%) were purchased from Merck (Darmstadt, Germany). 3,3′,5,5′-tetramethylbenzidine (TMB), 3-(4,5-dimethylthiazol-2-yl)-2,5-diphenyltetrazolium bromide (MTT), and the microbial culture media of Luria–Bertani (LB), Mueller–Hinton and blood agar were purchased from Sigma (Sigma-Aldrich, Germany). RPMI-1640 medium, fetal bovine serum (FBS), trypsin–EDTA solution, and antibiotic solution (penicillin–streptomycin) were obtained from Gibco (Invitrogen, Grand Island, NY).

## 2.2. Hydrothermal synthesis of CoFeCH NPs

CoFeCH NPs were synthesized by the hydrothermal method, according to a recently published article,[24] with some modifications. Briefly, 0.676 g $FeCl_3 \cdot 6H_2O$ and 0.297 g $CoCl_2 \cdot 6H_2O$ were added into 20 mL of ethylene glycol and stirred for 30 min to obtain a homogeneous mixture. 200 mg of CH and 1.8 g of sodium acetate were then added into the solution and stirred again for 30 min. The mixture was then transferred into a Teflon-lined autoclave, sealed and incubated at 150 °C for 8 h. After cooling to room temperature, the resultant colloids were separated magnetically and washed three times with distilled water to remove the unreacted chemicals, and the NPs were finally dried in an oven overnight at 60 °C. The uncoated CoFe NPs were also synthesized by the same method without the addition of CH.

## 2.3. Characterization of NPs

The size, morphology, and elemental composition of NPs were investigated by a field emission scanning electron micrometer (FE-SEM, FEI ESEM Quanta 200, USA) equipped with an X-ray energy dispersive spectrometer (EDS, silicon drift detectors, Germany) at an accelerating voltage of 25 kV. Fourier transform infrared (FTIR) spectroscopy (Jasco FTIR-6300, Tokyo, Japan) in the wavenumber range of 4000–400 $cm^{-1}$ was used to determine the functional surface groups of NPs. The crystal structure of NPs was characterized by a Bruker D-8 Advance powder X-ray diffractometer (Shimadzu, Japan) with Cu K$\alpha$ radiation ($\lambda$ = 1.5406 Å). The magnetic properties of NPs were evaluated using a vibrating sample magnetometer (VSM; Lake Shore Model 7400, Japan). The hydrodynamic size, particle size distribution, and zeta potential value of the NPs were determined by an SZ-100 nanoparticle analyzer (Horiba, Japan). A BELsorp-mini II instrument (Bel Japan Inc., Japan) was used to evaluate the nitrogen adsorption/desorption isotherms of the NPs. The surface area, pore size and pore volume of the NPs were calculated from the nitrogen desorption isotherms by the Brunauer–Emmett–Teller (BET) method and Barrett–Joyner–Halenda (BJH) model. Thermogravimetric analysis (TGA) of CoFe and CoFeCH NPs was performed using a Mettler TG50 (Schwerzenbach, Switzerland) under nitrogen atmosphere in the temperature range from 50 °C to 550 °C with a heating rate of 10 °C $min^{-1}$.

## 2.4. Antibacterial assays

The antibacterial activity of NPs was studied on Gram-positive *S. aureus* (ATCC25923) and Gram-negative *E. coli* (ATCC25922) bacterial species, according to the guidelines of the Institute of Clinical and Laboratory Standards.[25] Briefly, for the agar disk diffusion assay, the bacterial suspensions of *S. aureus* and *E. coli* were first prepared by the inoculation of a single colony in the nutrient broth and overnight incubation for 24 h at 30 °C and 37 °C, respectively. The turbidity of bacterial suspensions was then adjusted to 0.5 McFarland standards and inoculated on Mueller–Hinton agar (MHA) plates. The as-prepared filter paper discs of 6 mm in diameter were impregnated with 25 μg of NPs, and the reference antibiotics (amoxicillin and gentamicin) were then placed on the cultured plates. The as-prepared filter paper discs impregnated with 1–25 μg of CH were also used as the control. Finally, the inhibition zones were measured after 24 h incubation at the same condition. For the determination of the minimum inhibitory concentration (MIC), a serial dilution of NPs from 20 to $2 \times 10^3$ μg $mL^{-1}$ was done in sterile deionized water, and 100 μL of each dilution was added into each well of the 96-well microtiter plate containing 100 μL of 0.5 McFarland standard of the bacterial strain. After 18 h incubation, the bacterial growth was evaluated by measuring the absorbance of the wells at 630 nm using an Agilent 800TS ELISA reader. The most diluted well with no detectable absorbance was considered as MIC. The minimum concentration of NPs, which completely inhibits the bacterial growth (MBC), was determined by the subculture of MIC and neighboring wells on the blood agar and incubation for 18 h.

## 2.5. *In vitro* biocompatibility assays

The potential toxicity of NPs was studied on human umbilical vein endothelial cells (HUVEC) and human fibroblast (HFB)

cells using the MTT assay, according to a previous report.[26] Briefly, $10^4$ cells were seeded in each well of the 96-well plate and incubated overnight at 37 °C in a humidified 5% $CO_2$ incubator. The cells were then exposed to different concentrations of NPs (1, 10, 100, and 200 μg $mL^{-1}$) for 48 h. The medium was then removed, 100 μL of MTT solution (0.5 mg $mL^{-1}$ in media) was added into each well, and the cells were incubated again at 37 °C for 4 h. The medium was then carefully removed, and 100 μL of DMSO was added into each well to dissolve the formazan crystals. The viability of the cells was calculated as the ratio of the absorbance values from each treatment and the control at 570 nm.

### 2.6. Nanozyme activity of CoFe NPs

The peroxidase-like activity of NPs was studied in the presence of chromogenic TMB and $H_2O_2$ as a substrate, based on the previously reported method[5] with some modifications. The specific enzyme activity was determined using different concentrations of NPs and CH (5, 10, 15, 20, 25 μg $mL^{-1}$) with a fixed concentration of the substrates (1 M $H_2O_2$ and 20 mM TMB) in acetate buffer (0.2 M, pH 3.6). The constant concentration of NPs (10 mg $mL^{-1}$) with variable concentrations of the TMB substrate (10, 20, 50, 100, 150, 200, 250 mM) were also used to determine the enzyme kinetics. The absorbance of the reactions was monitored using a UV-vis spectrophotometer (Cary 100, Agilent, USA) at 652 nm. The catalytic activity was calculated based on the equation below.

$$C = \frac{V}{(\varepsilon \times l)} \times \left(\frac{\Delta A}{\Delta T}\right)$$

where $C$ is the catalytic activity of the nanozyme in units, $V$ is the volume of the reaction (mL), $\varepsilon$ is the molar absorbance coefficient of TMB (39 000 $M^{-1}$ $cm^{-1}$ at 652 nm), $l$ is the length of the cuvette cell (1 cm), and $\Delta A/\Delta T$ is the change in the absorbance of TMB at 652 nm per min. The specific activity was calculated based on the equation below

$$S = \frac{C}{M} = \frac{\frac{V}{(\varepsilon \times l)} \times \left(\frac{\Delta A}{\Delta T}\right)}{M}$$

where $S$ is the specific activity of the nanozyme (unit per mg) and $M$ is the concentration of NPs (mg).

### 2.7 Relaxivity measurement

A 1.5 T clinical MRI instrument (Siemens, Berlin, Germany) was used to investigate the ability of NPs as a $T_2$-weighted contrast agent. MRI signals were measured at different repetition times (TR) and the echo time (TE), including TR: 1500, 2000, 2500, 3000, 5000 ms and TE: 92 ms. For this purpose, a serial dilution containing different concentrations of Fe was prepared and used. The voxel signals were calculated using PACS software, and the $1/T_2$ of NPs was plotted linearly using the $R_2 = 1/T_2$ formula.

### 2.8. Statistical analyses

*In vitro* experiments were carried out in triplicate, and the results were expressed as the mean value of three independent experiments ± standard deviation. Student's *t*-test (Microsoft Excel, Microsoft Corporation, USA) was used to analyze the data, and $P$ values less than 0.05 were considered as statistically significant.

## 3 Results and discussion

### 3.1. Synthesis and characterization of NPs

A variety of analysis methods, including FE-SEM, EDS, BET, XRD, FTIR, TGA, VSM, and DLS, were used to fully characterize the hydrothermally-synthesized CoFeCH NPs. The SEM images (Fig. 1a) clearly show that the synthesized CoFeCH NPS are highly monodispersed and spherical with relatively similar sizes of about 20 nm. These results are consistent with the results of DLS analysis, which indicate the narrow size distribution of CoFeCH NPs with an average hydrodynamic size of 177.9 nm (Fig. S1†) and polydispersity index (PDI) of 0.238. The resultant CoFeCH NPs represent high colloidal stability with a zeta potential value of −33 (Fig. S2†), which could be attributed to the presence of carboxyl and hydroxyl groups on their surface. Interestingly, SEM imaging revealed that CH-coating significantly affect the size, morphology and dispersity of CoFe NPs compared to the uncoated NPs with a variety of shapes and sizes and significant agglomeration (Fig. 1a and d). Based on the EDS elemental analysis (Fig. S3†), CoFeCH NPs consist of Fe, Co, C, N, and O with the total weight percentages of 54.41, 15.04, 5.77, 6.67, and 18.1%, respectively. The presence of N in the composition of NPs confirmed the successful coating of NPs with CH. The XRD pattern of the powdered samples (Fig. 1b and e) showed the characteristic peaks located at 30.24°, 35.52°, 43.16°, 57.22°, and 62.68°, corresponding to the reflection planes of (220), (311), (400), (511), and (440), respectively, indexed to the cobalt iron oxide NPs with the formula $CoFe_2O_4$/CoO $Fe_2O_3$, according to the standard diffraction patterns of $CoFe_2O_4$ (JCPDS no. 22-1086). The significant peak located at $2\theta \approx 12°$ in the XRD pattern of CoFeCH NPs is attributed to the CH structure. The results of XRD analysis clearly showed the preserved crystal structure of CoFe NPs following the CH-coating.

CoFe NPs have attracted great attention due to their interesting magnetic properties, specially the excellent saturation magnetization, high coercivity, and magnetic susceptibility.[28] These NPs have found diverse applications in catalysis, biomedicine, as well as environmental remediation.[29] Therefore, the discovery of novel approaches to develop CoFe NPs with appropriate surface chemistry and superior magnetic activity is of great interest. The evaluation of the magnetic activity of CoFe and CoFeCH NPs using a VSM clarified their significant super-paramagnetic behavior with the saturation magnetization values of 69.31 and 59.37 emu $g^{-1}$ at room temperature, respectively (Fig. 1c and f). No hysteresis was observed in the hysteresis curve, and the remanence and coercivity were zero. The results also showed that the CH-coating of CoFe NPs reduced the magnetic activity of the resultant CoFeCH NPs. The excellent magnetic properties of CoFe nanospheres make them a promising alternative for biomedical applications, especially for imaging and magnetic separation.

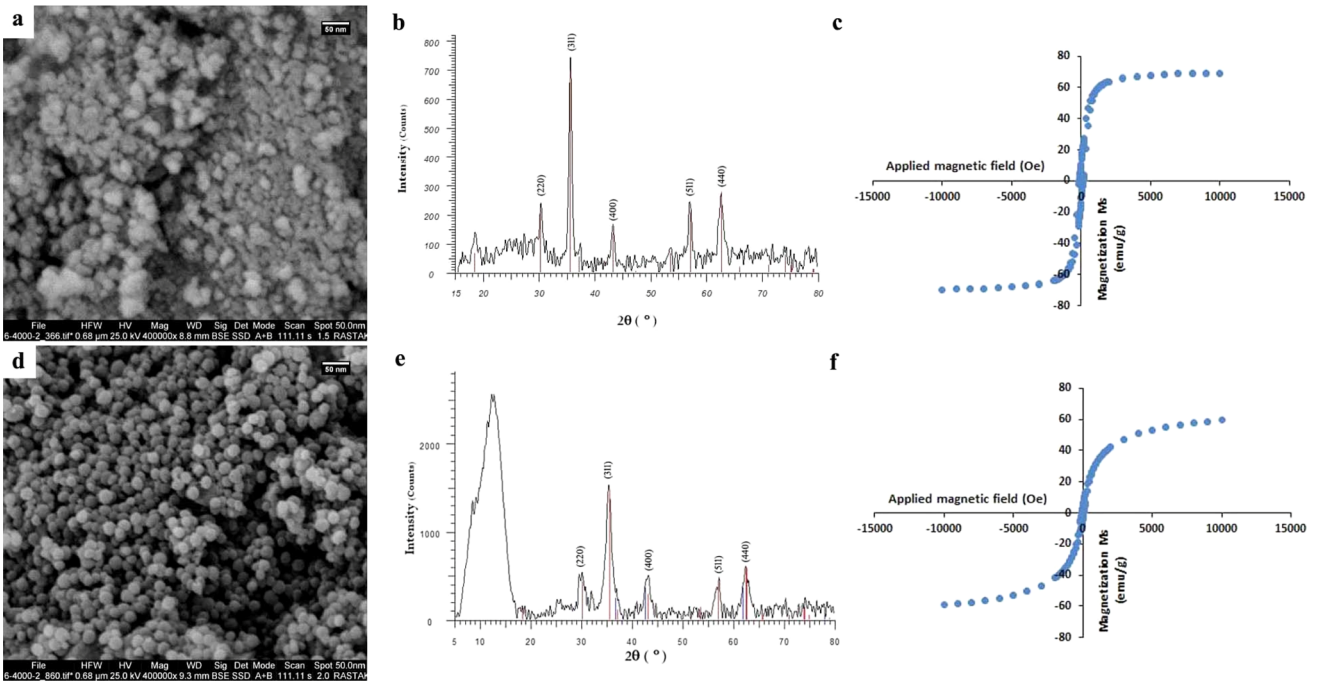


Fig. 1 SEM images (a and d), XRD patterns (b and e), and VSM curves (c and f) of CoFe (up) and CoFeCH (down) NPs.

The FTIR spectra of CoFe and CoFeCH NPs (Fig. 2a) clearly show the stretching vibration band of Fe–O at 575 $cm^{-1}$. The peaks at 1052 and 1337 $cm^{-1}$ are attributed to the C–O and N–H stretching vibrations of CH, respectively,[27] which confirm the successful CH-coating of NPs. The TGA results (Fig. 2b) show a weight loss of 9.6 wt% for CoFe NPs when the temperature increased to 550 °C. At the same condition, a total weight loss of 26.4 wt% was obtained for CoFeCH NPs when the temperature increased from 50 °C to 550 °C, indicating that about 16.8 wt% of CoFeCH NPs consists of CH. The results of TGA analysis further confirmed the efficient CH-coating of CoFe NPs, in accordance with the results of FE-SEM, FTIR, and XRD analysis. $N_2$ adsorption–desorption analysis was also used to evaluate the BET surface area and the mesoporous structure of CoFeCH NPs. The results (Fig. 2c) confirm the mesoporous structure of CoFeCH NPs with a type IV isotherm. The calculated specific surface area from the BET plot for CoFeCH NPs is 89.583 $m^2$ $g^{-1}$, which is significantly higher than that of uncoated NPs with 68.121 $m^2$ $g^{-1}$. The pore-size distribution spectra obtained by the BJH model for the CoFe and CoFeCH NPs (Fig. 2d) also showed a significant difference between NPs with or without CH-coating. The observed narrow range mesopores of 1–20 nm in CoFe NPs is attributed to the microspheres formed by the stacking of NPs.[28] The total pore volume of NPs also increased from 0.2457 to 0.3668 $cm^3$ $g^{-1}$ after CH-coating. These results indicate the high potential of mesoporous CoFeCH NPs as a carrier for magnetically-targeted drug delivery.

### 3.2. Antibacterial activity of NPs

The use of organic compounds for the surface functionalization of NPs is an attractive approach to obtain highly colloidal NPs with novel or superior biological properties.[30] Therefore, surface functionalization using CH, with the well-known antimicrobial effects, is expected to improve the antimicrobial activity of CoFe NPs. To confirm this assumption, the potential antibacterial effects of CoFe and CoFeCH NPs were studied on *E. coli* and *S. aureus* bacteria.

Fig. 4 shows the growth inhibition zones of *S. aureus* and *E. coli* bacteria following exposure with CoFe and CoFeCH NPs as well as reference antibiotics. The results clearly show the significant antibacterial effects of NPs on both bacterial strains. Growth inhibition zones with diameters of 25.8 ± 1.4 mm and 30.1 ± 1.9 mm were obtained for *S. aureus* after 18 h incubation with the filter discs impregnated with 25 μg of CoFe and CoFeCH NPs, respectively. Incubation with amoxicillin under the same conditions led to an inhibition zone of 13.1 ± 1.2 mm in diameter (Fig. 3a). Interestingly, these results indicate that CoFeCH NPs display significantly higher antibacterial activity than uncoated NPs and the reference antibiotic amoxicillin. The antibacterial activity of different concentrations (1–25 μg) of CH as the control sample was also studied on *S. aureus* and *E. coli* bacteria. While no growth inhibition was observed for *E. coli*, growth inhibition zones of diameter 7.8, 8.9 and 10.1 mm were obtained for *S. aureus* after 18 h incubation with the filter discs impregnated with 5, 10, and 25 μg of CH, respectively. The results indicated that the CH-coating of CoFe significantly increased their antibacterial activity.

CoFe and CoFeCH NPs also showed significant antibacterial effects on *E. coli*. The growth inhibition zones of 17.6 ± 1.3 mm and 22.7 ± 2.9 mm in diameter were obtained with 25 μg of CoFe and CoFeCH NPs, respectively, while a growth inhibition zone of 27.1 ± 1.6 mm was obtained for gentamicin under the

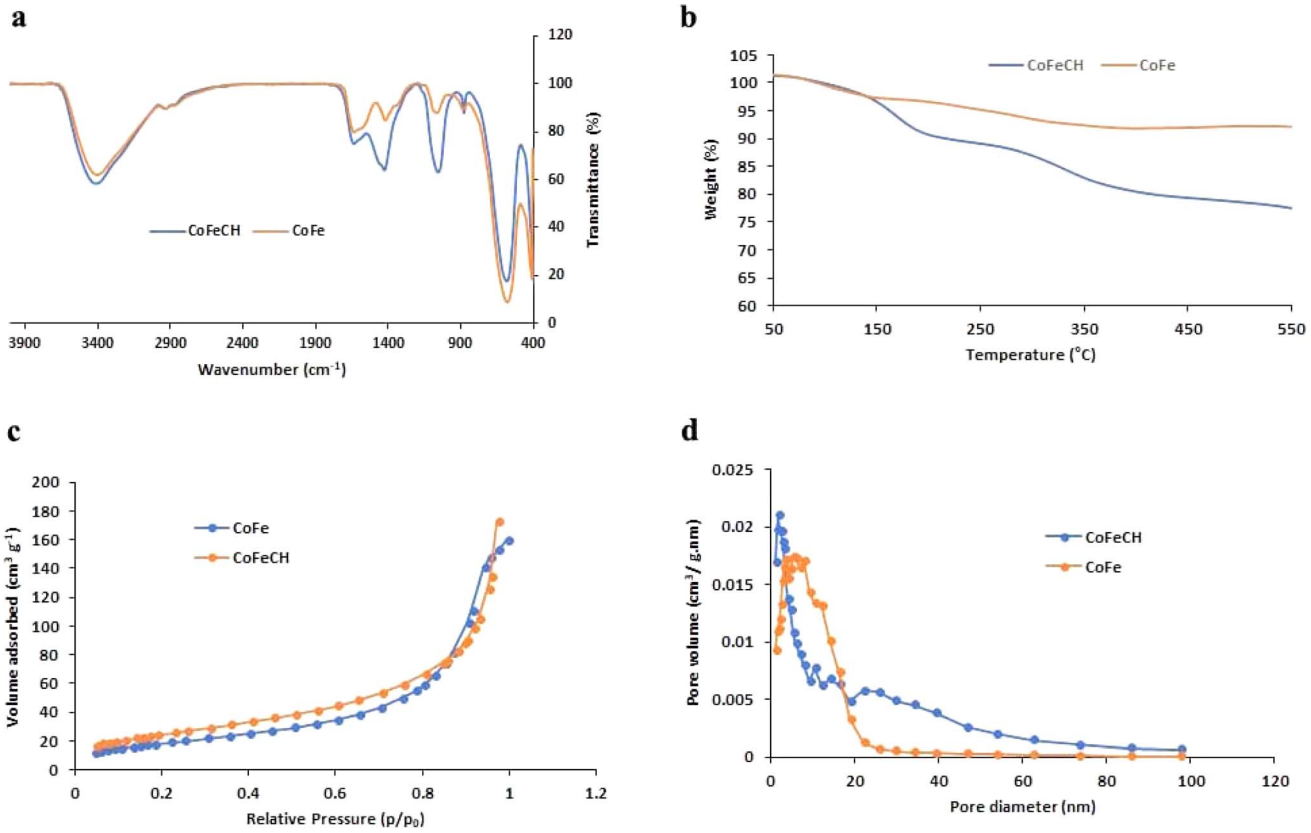


Fig. 2 FTIR spectra (a), TGA curves (b), $N_2$ adsorption/desorption isotherms (c), and Barrett–Joyner–Halenda (BJH) pore size distribution plots (d) of CoFe and CoFeCH NPs.

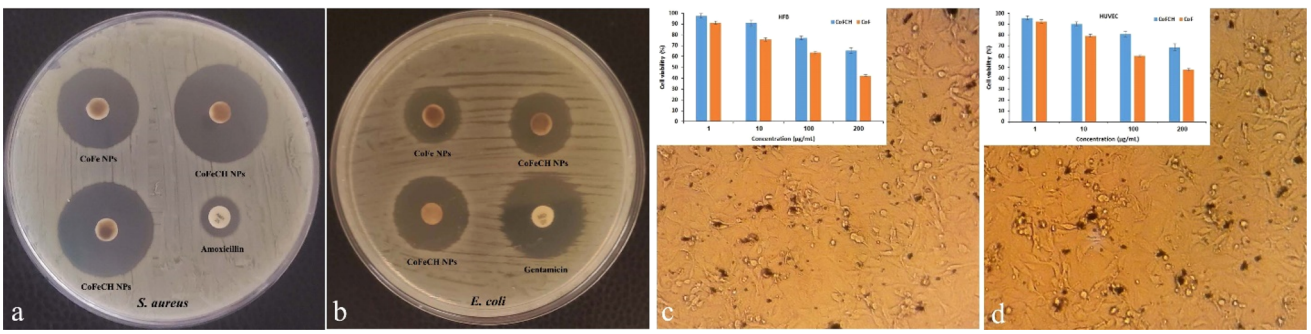


Fig. 3 The growth inhibition zones of *S. aureus* (a) and *E. coli* (b) after incubation with 25 μg of NPs and antibiotics. The morphology of HFB (c) and HUVEC (d) cells after exposure with 100 μg of CoFeCH NPs. The insets show the cell viability percentages after exposure with different concentrations of NPs.

same conditions (Fig. 3b). These results also confirmed the considerable effect of CH-coating on the improved antibacterial activity of CoFe NPs. Table 1 illustrates the MIC values of NPs on *S. aureus* and *E. coli* cells. The results, in agreement with the results of the antibiogram test, indicate the higher antibacterial effects of CoFeCH NPs on *E. coli* cells, but no significant difference is observed in the antibacterial activity of CoFe and CoFeCH NPs on *S. aureus* bacteria. These results clearly show the high potential of CoFeCH NPs as an alternative to

Table 1 MIC and MBC values of CoFe and CoFeCH NPs on *E. coli* and *S. aureus*

| Antibacterial activities (μg mL$^{-1}$) | *E. coli* | | *S. aureus* | |
|---|---|---|---|---|
| | MIC | MBC | MIC | MBC |
| CoFe NPs | 160 | 320 | 80 | 160 |
| CoFeCH NPs | 80 | 320 | 80 | 160 |

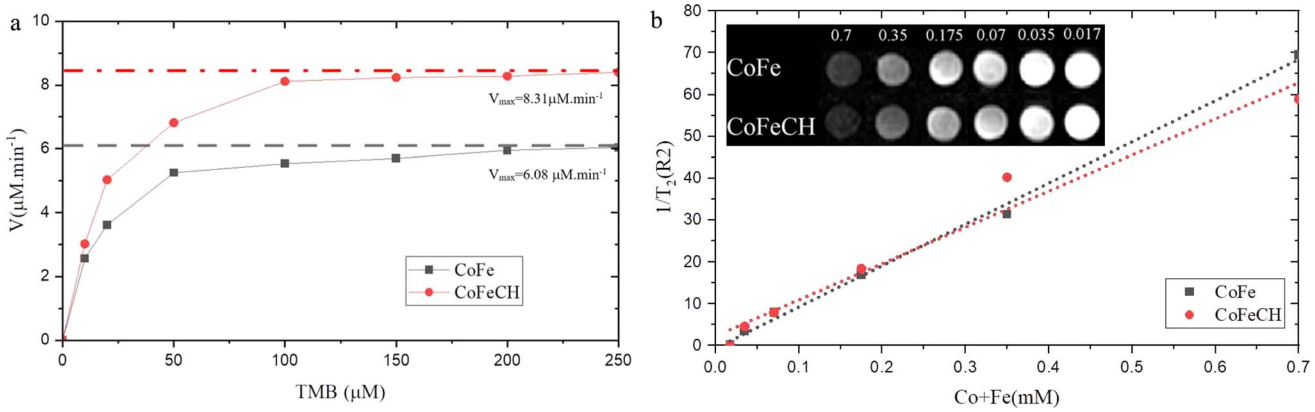


Fig. 4 Michaelis–Menten curves of CoFe and CoFeCH NPs (a). $1/T_2$ (transverse relaxation rate) of CoFe and CoFeCH NPs at different concentrations (b), and $T_2$-weighted image of wells containing CoFe and CoFeCH NPs with different concentrations from 0.7 to 0.017 mM (inset).

commonly used antibiotics. According to the literature, the observed antibacterial effects of CoFeCH NPs could be mainly attributed to the generation of ROS, the cell wall and membrane damages due to the physical interactions, leaching and dissolution of $Co^{2+}$ ions, and CH-mediated effects.[19,31] The results are comparable with those reported previously.[15,32,33]

### 3.3. *In vitro* biocompatibility studies

Regarding the intrinsic cytotoxicity of CoFe NPs,[13] the surface coating of NPs in order to improve their biocompatibility is essential before biomedical applications. The effect of CH-coating on the biocompatibility of CoFe NPs was evaluated on HUVEC and HFB cells *in vitro*. The results (Fig. 3c and d) clearly showed the significantly higher biocompatibility of CH-coated NPs compared to the uncoated NPs. The NPs represented a concentration-dependent cytotoxicity on both the cell lines. While 60.75 and 63.71% of HUVEC and HFB cells were viable after 48 h exposure to 100 μg $mL^{-1}$ of CoFe NPs, viability percentages of 76.92 and 80.7% were obtained for HUVEC and HFB cells, respectively, in the presence of CoFeCH NPs under the same conditions. The monitoring of the cell morphology also confirmed the results of the MTT assay (Fig. 3c and d). The effect of CH-coating on the improved biocompatibility of CoFe NPs synthesized by the chemical coprecipitation method has also been reported by Shakil *et al.*, recently.[14] The biocompatibility and magnetic heating efficiency of CoFe NPs coated physically with CH have also been reported by Phong *et al.*[27]

### 3.4. Peroxidase like activity

Recently, the development of NPs with peroxidase-mimicking activity has attracted increasing attention in modern biotechnology owing to their extensive applications in labeling and biosensing.[34] CoFe NPs have also been reported to display the intrinsic peroxidase-like activity.[7] Regarding the significant effect of size, morphology, composition and surface chemistry on the enzyme activity of NPs,[35] the peroxidase-like activity of CoFeCH NPs was studied and compared with CoFe NPs. For this purpose, the ability of NPs to catalyze the $H_2O_2$-mediated oxidation of TMB was studied by monitoring the absorbance of the reaction mixture at 652 nm. The results (Fig. 4a) show the higher peroxidase activity of CoFeCH NPs compared to the uncoated NPs. The $K_m$ values of 15.88 mM and 14.37 were obtained for CoFe and CoFeCH NPs, respectively, which indicate the higher affinity of CoFeCH NPs for the TMB. The specific activities of 0.501 and 0.632 mmol $min^{-1}$ were also obtained for CoFe and CoFeCH NPs, respectively. Under the same conditions, no peroxidase-like activity was obtained for different concentrations (5–25 μg $mL^{-1}$) of CH.

### 3.5. Relaxivity measurement

CoFe NPs have also been considered as a potent MRI contrast agent recently. Therefore, the potential use of CoFe and CoFeCH NPs for MRI imaging was also studied. The results (Fig. 4b) show a significant decrease in the emitted signal from voxel with the increase in Fe concentration from 1 to 100. The $R_2$ values of 97.4 and 91.3 $mM^{-1}$ $s^{-1}$ were also obtained for CoFe and CoFeCH NPs, respectively, indicating a slight reduction in the magnetic intensity due to the CH-coating (Fig. 4b). The results are comparable with the transverse relaxation rate of 81.1 $mM^{-1}$ $s^{-1}$ reported recently by Poorhossein *et al.*, for PEG-coated CoFe NPs.[36]

## 4 Conclusion

The magnetic and catalytic activities of CoFe NPs have attracted great attention recently for different biomedical applications. However, the facile and large-scale synthesis of highly colloidal and monodispersed CoFe NPs without cytotoxic effects is an important limitation to their extensive applications. In this study, CoFe NPs with CH-coating were synthesized in one step using a hydrothermal method. The resultant CoFeCH NPs represent a spherical shape, high monodispersity and colloidal stability, mesoporous and crystalline structure, and significant magnetic activity.

The CH-functionalization of CoFe NPs improved their biocompatibility on human cells as well as their antibacterial

effects on *S. aureus* and *E. coli*. The CoFeCH NPs also display significant peroxidase-like activity that could be used for the development of biosensors. The appropriate biocompatibility and magnetic activity of CoFeCH NPs make them a potent MRI contrast agent. Therefore, the overall results clearly indicated the significant effect of CH-coating on the monodispersity, biocompatibility, porosity, enzymatic and antibacterial activity of CoFe NPs. In conclusion, the synthesized CoFeCH NPs could be suggested for different biomedical applications, especially as an antibacterial and contrast agent as well as a nanocarrier for targeted drug delivery.

## Abbreviations

| | |
|---|---|
| BET | Brunauer–Emmett–Teller |
| BJH | Barrett–Joyner–Halenda |
| CH | Chitosan |
| CoFe | Cobalt ferrite |
| CoFeCH | CH-coated CoF |
| DLS | Dynamic light scattering |
| DD | Degree of deacetylation |
| DMSO | Dimethyl sulfoxide |
| EDS | Energy dispersive X-ray spectroscopy |
| FBS | Fetal bovine serum |
| FE-SEM | Field emission scanning electron microscopy |
| FTIR | Fourier transform infrared spectroscopy |
| HFB | Human fibroblast |
| HUVEC | Human umbilical vein endothelial cells |
| LB | Luria–Bertani |
| MBC | Minimum bactericidal concentration |
| MDR | Multiple drug resistance |
| MHA | Mueller–Hinton agar |
| MIC | Minimum inhibitory concentration |
| MRI | Magnetic resonance imaging |
| NPs | Nanoparticles |
| PDI | Polydispersity index |
| PEG | Polyethylene glycol |
| RPMI | Roswell park memorial institute |
| ROS | Reactive oxygen species |
| SD | Standard deviation |
| TE | Echo time |
| TGA | Thermogravimetric analysis |
| TMB | 3,3′,5,5′-Tetramethylbenzidine |
| TR | Repetition times |
| UV-vis | Ultraviolet-visible |
| VSM | Vibration sample magnetometer |
| XRD | X-ray diffraction |

## Author contributions

Abolghasem Abbasi Kajani: conception, design, analysis and writing of the study. Ali Pouresmaeili: analysis and writing of the study. Mehdi Kamali: analysis and writing of the study.

## Conflicts of interest

The authors declare no conflict of interest.

## Acknowledgements

The financial supports of University of Isfahan are gratefully acknowledged.

## References

1 N. Baig, I. Kammakakam, W. Falath and I. Kammakakam, *Mater. Adv.*, 2021, **2**, 1821–1871.
2 K. Fan, J. Xi, L. Fan, P. Wang, C. Zhu, Y. Tang, X. Xu, M. Liang, B. Jiang, X. Yan and L. Gao, *Nat. Commun.*, 2018, **9**, 1440.
3 M. Chen, H. Zhou, X. Liu, T. Yuan, W. Wang, C. Zhao, Y. Zhao, F. Zhou, X. Wang, Z. Xue, T. Yao, C. Xiong and Y. Wu, *Small*, 2020, **16**, 1–6.
4 H. Ding, Y. Cai, L. Gao, M. Liang, B. Miao, H. Wu, Y. Liu, N. Xie, A. Tang, K. Fan, X. Yan and G. Nie, *Nano Lett.*, 2019, **19**, 203–209.
5 B. Jiang, D. Duan, L. Gao, M. Zhou, K. Fan, Y. Tang, J. Xi, Y. Bi, Z. Tong, G. F. Gao, N. Xie, A. Tang, G. Nie, M. Liang and X. Yan, *Nat. Protoc.*, 2018, **13**, 1506–1520.
6 Z. Wang, R. Zhang, X. Yan and K. Fan, *Mater. Today*, 2020, **41**, 81–119.
7 K. Zhang, W. Zuo, Z. Wang, J. Liu, T. Li, B. Wang and Z. Yang, *RSC Adv.*, 2015, **5**, 10632–10640.
8 Y. Peng, Z. Wang, W. Liu, H. Zhang, W. Zuo, H. Tang, F. Chen and B. Wang, *Dalton Trans.*, 2015, **44**, 12871–12877.
9 A. A. P. Mansur, H. S. Mansur and S. M. Carvalho, *Catal. Today*, 2022, **388–389**, 187–198.
10 G. Wei, X. Liang, Z. He, Y. Liao, Z. Xie, P. Liu, S. Ji, H. He, D. Li and J. Zhang, *J. Mol. Catal. A: Chem.*, 2015, **398**, 86–94.
11 D. Jiang, D. Ni, Z. T. Rosenkrans, P. Huang, X. Yan and W. Cai, *Chem. Soc. Rev.*, 2019, **48**, 3683–3704.
12 M. A. Dheyab, A. A. Aziz, M. S. Jameel, O. A. Noqta, P. M. Khaniabadi and B. Mehrdel, *Sci. Rep.*, 2020, **10**, 1–8.
13 H. Zhang, J. Wang, Y. Zeng, G. Wang, S. Han, Z. Yang, B. Li, X. Wang, J. Gao, L. Zheng, X. Liu, Z. Huo and R. Yu, *Phys. Lett. A: Gen. At. Solid State Phys.*, 2020, **384**, 126600.
14 M. S. Shakil, M. A. Hasan, M. F. Uddin, A. Islam, A. Nahar, H. Das, M. N. I. Khan, B. P. Dey, B. Rokeya and S. M. Hoque, *ACS Appl. Bio Mater.*, 2020, **3**, 7952–7964.
15 D. Gingasu, I. Mindru, L. Patron, A. Ianculescu, E. Vasile, G. Marinescu, S. Preda, L. Diamandescu, O. Oprea, M. Popa, C. Saviuc and M. C. Chifiriuc, *J. Inorg. Organomet. Polym. Mater.*, 2018, **28**, 1932–1941.
16 A. K. Chaurasia, N. D. Thorat, A. Tandon, J. H. Kim, S. H. Park and K. K. Kim, *Sci. Rep.*, 2016, **6**, 1–13.
17 L. Mei, S. Zhu, Y. Liu, W. Yin, Z. Gu and Y. Zhao, *Chem. Eng. J.*, 2021, **418**, 129431.
18 L. M. Streicher, *J. Global Antimicrob. Resist.*, 2021, **24**, 285–295.
19 L. Wang, C. Hu and L. Shao, *Int. J. Nanomed.*, 2017, **12**, 1227–1249.
20 J. Zhang and J. Liu, *Nanoscale*, 2020, **12**, 2914–2923.
21 S. Shaikh, N. A. Lapin, B. Prasad, C. R. Sturge, C. Pybus, R. Pifer, Q. Wang, B. M. Evers, R. Chopra and D. E. Greenberg, *Sci. Rep.*, 2023, **13**, 1–12.

22 J. Robertson, *Am. Math. Mon.*, 2004, **111**, 915.
23 A. Abbasi Kajani and M. A. Mehrgardi, *Nanomedicine*, 2021, **16**, 627–639.
24 A. Ayub, B. Kim, Y. Lim, K. C. Devarayapalli, G. Kim and D. S. Lee, *J. Alloys Compd.*, 2023, **963**, 171294.
25 Clinical and Laboratory Standards Institute (CLSI), *Ref. Method Broth Dilution Antifung. Susceptibility Test. Yeasts. Approv. Stand*, 3th edn, 2008, vol. 28, p. 13.
26 A. Abbasi Kajani, A. K. Bordbar, S. H. Zarkesh-Esfahani, A. Razmjou and J. Hou, *J. Mol. Liq.*, 2017, **247**, 238–245.
27 P. H. Nam, N. X. Phuc, D. H. Manh, D. K. Tung, V. Q. Nguyen, N. H. Nam, P. K. Son, T. N. Bach and P. T. Phong, *Phys. E*, 2021, **134**, 114862.
28 M. P. Reddy, A. M. A. Mohamed, X. B. Zhou, S. Du and Q. Huang, *J. Magn. Magn. Mater.*, 2015, **388**, 40–44.
29 N. Chaibakhsh and Z. Moradi-Shoeili, *Mater. Sci. Eng., C*, 2019, **99**, 1424–1447.
30 A. Abbasi Kajani and A. K. Bordbar, *J. Hazard. Mater.*, 2019, **366**, 268–274.
31 D. Franco, G. Calabrese, S. P. P. Guglielmino and S. Conoci, *Microorganisms*, 2022, **10**, 1778.
32 M. I. A. A. Maksoud, G. S. El-Sayyad, A. H. Ashour, A. I. El-Batal, M. A. Elsayed, M. Gobara, A. M. El-Khawaga, E. K. Abdel-Khalek and M. M. El-Okr, *Microb. Pathog.*, 2019, **127**, 144–158.
33 D. Gheidari, M. Mehrdad, S. Maleki and S. Hosseini, *Heliyon*, 2020, **6**, e05058.
34 M. A. Komkova, E. E. Karyakina and A. A. Karyakin, *J. Am. Chem. Soc.*, 2018, **140**, 11302–11307.
35 M. Raineri, E. L. Winkler, T. E. Torres, M. V. Mansilla, M. S. Nadal, R. D. Zysler and E. Lima, *Nanoscale*, 2019, **11**, 18393–18406.
36 M. Poorhossein, F. Pishbin, A. Ataie and M. Akrami, *Ceram. Int.*, 2023, **49**, 2705–2714.